Evidence for efficient non-evaporative leaf-to-air heat dissipation in a pine forest under drought conditions

Jonathan D. Muller[1,*], Eyal Rotenberg[1], Fyodor Tatarinov[1], Itay Oz[1], and Dan Yakir[1]

[1]Department of Earth and Planetary Sciences, Weizmann Institute of Science, 7610001 Rehovot, Israel
[*]*Corresponding author: jonathan.muller@weizmann.ac.il*

February 2021

Abstract

- Drier climates predicted for many regions can result in reduced evaporative cooling leading to overheating of leaves and enhanced mortality. To what extent non-evaporative cooling can contribute to plant resilience to the increasingly stressful conditions is poorly known at present.
- Using a novel, high accuracy infrared system for continuous measurements of leaf temperature in mature trees under field conditions, we assessed leaf-to-air temperature differences $\Delta T_{leaf-air}$ of pine needles during drought.
- $\Delta T_{leaf-air}$ was weakly related to variations in the radiation load and wind speed, but highly dependent on canopy structure and within-canopy turbulence that enhance the sensible heat flux H. On mid-summer days, $\Delta T_{leaf-air}$ remained around 2 °C, both in trees exposed to summer drought, and in those provided with a supplement irrigation having a 10x higher transpiration rate. The non-evaporative cooling in the drought-exposed trees must be facilitated by low resistance to heat transfer generating large H.
- Non-evaporative cooling is demonstrated as an effective cooling mechanism in needle-leaf trees, which can be a critical factor in forest resistance to drying climates. The generation of large H at the leaf scale provides a basis for the development of the previously identified canopy-scale heat dissipation through the 'convector effect'.

1 Introduction

In hot and dry ecosystems where plants operate near their limits, maintaining leaf temperature below their thermal threshold (41.5–50.8 °C depending on species and climate zone; O'sullivan et al., 2017) is critical. Indeed, high temperatures can affect a variety of biophysical and biochemical processes (Still et al., 2019; Baldocchi and Penuelas, 2019) like photosynthesis, where they are associated with damage to the functioning of photosystems I & II or the carbon reduction cycle (O'sullivan et al., 2017; Maseyk, 2006; Long et al., 1994; Werner et al., 2002), or an increased vapour pressure deficit and stomatal closure (Smith, 1980; Richardson et al., 2020). Not surprisingly, there has been a substantial increase in reports of drought-related tree mortality with rising air temperatures (Allen et al., 2010, 2015).

Biosphere-atmosphere interactions affect local and global climatic conditions by influencing ecosystem gas and energy fluxes (Bonan, 2008). These highly depend on leaf surface temperature, hence the need to accurately estimate it and its variability. In dry conditions, excess energy absorbed from incoming radiation cannot be readily

dissipated through latent heat (transpiration) due to constraints on water availability. Alternatively, excess energy can be converted to sensible heat which has previously been shown to lead to a canopy 'convector effect' that dissipates heat from the ecosystem to the atmospheric boundary layer (Rotenberg and Yakir, 2010; Banerjee et al., 2017; Zhang et al., 2019). Yet, understanding the evolution of this mechanism at the leaf scale, and the regulation of leaf temperature, and to what degree climatic changes could push leaves over their physiological limits and enhance mortality is poorly known at present (Still et al., 2019).

Leaf cooling through sensible heat is highly dependent on the coupling of leaves and their surrounding air. Indeed, leaf-to-air temperature difference $\Delta T_{leaf-air}$ is often used as stress indicators in agricultural crops (Kim et al., 2018; Maimaitijiang et al., 2020; Zhang et al., 2019; Song et al., 2017; Long et al., 2006). A wide range of factors can influence leaf-to-air heat transfer, including land cover type, atmospheric conditions, soil temperature and moisture, short- and longwave radiation inputs as well as elevation and latitude (Bonan, 2008; Still et al., 2019; Kim et al., 2016). These factors affect both the amount of absorbed energy and the penetration of wind into the canopy layer. The interplay between wind and leaf temperature is complex: on the one hand, it can increase leaf water loss because of the transport of moist air away from leaves (Schymanski and Or, 2016; McMahon et al., 2013; Neriah et al., 2014), which increases evaporative cooling. On the other hand, wind can transport sensible heat away from leaves, providing an air cooling mechanism that can decrease water loss, since transpiration is a function of leaf temperature (Schymanski and Or, 2016). Overall, this mechanism is expected to be species-dependent since the reduction in resistance to sensible heat transfer through efficient air flow scales with reduced leaf dimensions (Schymanski and Or, 2016; Taylor, 1975; Geller and Smith, 1982). Indeed, leaf size has been shown to be an important factor affecting leaf-to-air heat transfer due to its effect on the leaf boundary layer (Leuzinger and Körner, 2007; Schymanski and Or, 2016): thin leaves such as those found in conifers have a much lower $\Delta T_{leaf-air}$ of 4–8 °C compared to broadleaf species, where $\Delta T_{leaf-air}$ reached 10–15 °C (Kim et al., 2018; Jones, 2004), even in temperate climates where the daytime air temperature rarely exceeds 25°C (see literature value review in Table S7.1). In agricultural studies, $\Delta T_{leaf-air}$ was shown to depend on soil moisture due to the ability of plants to evaporate more water (Siebert et al., 2014). However, since the seminal work of Kim et al. (2016) on ponderosa pine canopies, few studies have followed up on climatic effects on leaf temperature on trees under field conditions, even less so in xeric ecosystems (Lapidot et al., 2019). Furthermore, we are presently unaware of any studies measuring $\Delta T_{leaf-air}$ across the height of a canopy, or comparisons between non-water-limited trees that rely on evaporative cooling versus drought-exposed trees that are limited to air-cooling in field conditions.

High precision, direct measurements of leaf temperature under field conditions are a prerequisite to extend our knowledge in this area, but they remain rare (see reviews in (Still et al., 2019; Aubrecht et al., 2016). This is particularly so in forests due to the vegetation height and because of the required combined measurement of leaf surface temperatures and that of the surrounding air (Kim et al., 2018). In many studies, thermocouples were used in spite of their limitations, i.e., the radiative and convective heat exchange of the thermocouple junction with the environment owing to exposure of most of the thermocouple junction to the air, and a poor connection between the junction and the leaf surface (Tarnopolsky and Seginer, 1999; Pieters and Schurer, 1973), a factor which applies especially to needle-leaves. Several studies have chosen infrared thermography for leaf temperature (Still et al., 2019; Jones, 2004). Yet, remaining challenges in using these sensors are the required calibration, knowledge of leaf emissivity (Richardson et al., 2020; Idso et al., 1969) and of background thermal radiation coming from all ecosystem elements (soil, plants, atmosphere). In most studies, emissivity is taken from literature values, but complication associated with physiological effects such as changes in emissivity during leaf emergence or differences between species can lead to measurement inaccuracies of up to 3 °C (Richardson et al., 2020). Furthermore, background thermal radiation has sometimes either been ignored or simplified using air temperature as a substitute (Birami et al., 2018). This is based on the assumption of a small error due to the high emissivity of natural materials (>0.95), assumptions that are not always warranted (Kim

et al., 2016). Alternatively, background thermal radiation has been measured using independent sensors (Aubrecht et al., 2016), or empirical correction equations were developed (Kim et al., 2018) using other environmental variables such as air temperature and/or relative humidity (Birami et al., 2018). Nevertheless, these methods can lead to substantial measurement errors of up to several degrees, which can be critical in comparing leaf-to-air temperature of similar magnitudes under field conditions. To our knowledge, air temperature has not previously been measured in the vicinity of leaves, thus amplifying the error of these measurements.

In this study, our objectives were: (a) to develop and apply a sufficiently accurate method to measure $\Delta T_{leaf-air}$ under field conditions in needle-leaves; (b) to examine the spatial (across canopy height) and temporal (diurnal) variations of $\Delta T_{leaf-air}$ in the absence of evaporative cooling under drought, or when it is kept high by supplemental irrigation. We hypothesized, first, that an efficient non-evaporative cooling at the leaf scale can prevent leaf overheating under high temperature and radiation load in trees growing under dry conditions, and second, that this requires the generation of a high sensible heat flux, which could underlie the canopy-scale heat dissipation via the so-called 'convector effect', providing resilience to forests undergoing warming and drying climatic trends.

2 Materials & Methods

2.1 Site description & meteorological measurements

The Yatir forest research site is located in a 2800 ha afforestation of mainly *Pinus halepensis* trees in the dry southern Mediterranean region, at the northern edge of the Negev desert in Israel (31°20′49″N; 35°3′7″E; altitude 600–850 m above sea level). Tree density was 300 trees ha^{-1}, corresponding to ~50 % crown cover, mean annual global radiation was 238 W m^{-2}, while average air temperatures for January and July are 10 and 25.8 °C respectively, with a mean annual potential ET of 1600 mm, and mean annual precipitation of 285 mm (Rotenberg and Yakir, 2010; Tatarinov et al., 2016; Qubaja et al., 2019). Measurements were done during the extended dry season (June to October) typical for the semi-arid southern Mediterranean climate zone.

The research site contains an eddy covariance flux tower operating since 2000, whose above-canopy environmental sensors (15 m agl; air temperature (°C), RH (%), wind speed at 18.7 m agl (m s^{-1}); R3-100, Gill Instruments, Lymington, United Kingdom), shortwave (0–4000 nm (W m^{-2}); CM21, Kipp & Zonen B.V., Delft, The Netherlands) and longwave radiation (4–50 µm (W m^{-2}); Eppley, Newport RI) were used for auxiliary measurements of meteorological conditions during our consecutive measurement periods (Table 1) on a half-hourly timescale.

Midday conditions (10:00-14:00) were similar during the consecutive measurement periods: air temperatures were ~31 °C, above-canopy incoming short- and longwave radiation were ~929 and 362 W m^{-2}, respectively, while above-canopy wind speed averaged 3.22 m s^{-1} and VPD 2.72 kPa. These values, summarized in Table 1, show that conditions during summer drought remain stable and comparable, even though measurements were not taken simultaneously.

Finally, measurements from an experimental plot active since the spring of 2016 were available, where gas exchange chambers were used to measure assimilation and transpiration of multiple leaves on 4 twigs per chamber under summer supplemental irrigation and drought-exposed (i.e., control) conditions (Preisler, 2019).

2.2 Leaf and air temperature: Measurement principles

Thermal infrared cameras pick up thermal radiation from different sources: first, that emitted by the object of interest L_{obj} with emissivity ε_{obj}. Second, the radiation of the surrounding background L_{bg} that the object reflects according to $1-\varepsilon_{obj}$ (with both object and reflected radiation attenuated through the air column by a transmissivity coefficient τ). Third, the thermal radiation of the air column L_{air} between the sensor and the object emitting according to $1-\tau$, which

Table 1. Midday conditions (10:00-14:00) during consecutive measurements of leaf temperatures in summers 2018 & 2019 with standard deviations, showing conditions in the experimental height ('exp') and in the atmosphere, measured above canopy ('atm') in 15m agl. Performed experiments were measurements in different heights in 2018, and in an irrigated and drought-exposed plot in 2018 & 2019. Columns show the experiment (Exp), year and exact dates of measurements, height above ground level, air temperature T_{air} [°C], incoming solar and longwave thermal radiation above canopy S_{atm} [W m^{-2}] Φ_{air} [W m^{-2}], respectively, longwave radiation in the experimental height L_{exp} [W m^{-2}], wind speed above canopy and in the experimental height u_{atm} [m s^{-1}] and u_{exp} [m s^{-1}], respectively and mean leaf-to-air temperature difference $\Delta T_{leaf-air}$ [°C]

Exp.	Year	Dates	Height agl [m]	T_{air} [°C]	S_{atm} [W m^{-2}]	L_{atm} [W m^{-2}]	L_{exp} [W m^{-2}]	u_{atm} [m s^{-1}]	u_{exp} [m s^{-1}]	$\Delta T_{leaf-air}$ [°C]
Heights	2018	05.07.–19.07.	3.00	31.18 (1.89)	978.25 (62.09)	355.60 (11.95)		3.31 (0.60)	0.82 (0.13)	3.23 (0.65)
		20.07.–30.07.	5.00	30.53 (2.75)	935.29 (87.65)	366.69 (11.52)	455.60 (16.23)	3.66 (0.66)	0.81 (0.13)	2.16 (0.46)
		14.08.–27.08.	7.00	30.64 (1.95)	913.90 (89.92)	360.63 (14.79)		3.14 (0.75)	0.75 (0.18)	1.78 (0.86)
		01.08.–13.08.	8.50	31.01 (1.81)	933.65 (95.00)	363.82 (13.05)		3.42 (0.82)	0.87 (0.21)	1.14 (0.41)
Irrigation	2018	29.08.–14.09.	4.75	31.22 (2.78)	841.39 (94.30)	368.49 (13.40)	464.68 (14.36)	2.83 (0.90)	0.63 (0.12)	1.89 (1.40)
	2019	01.07.–31.07.	5.75	31.62 (2.28)	973.01 (56.46)	357.96 (14.28)	468.86 (15.03)	3.09 (0.92)	0.90 (0.25)	1.79 (1.19)
Drought-exposed	2018	01.07.–30.07.	5.00	30.80 (2.48)	946.69 (78.91)	363.24 (12.47)	454.46 (14.89)	3.34 (0.82)	0.84 (0.15)	2.30 (0.52)
	2019	31.07.–14.09.	5.00	31.14 (2.27)	910.72 (91.70)	362.77 (14.76)	488.91 (16.42)	2.96 (0.84)	0.64 (0.16)	3.51 (0.65)

is affected by the air temperature, humidity and aerosols content (Fig. 1). Hence, the total measured longwave radiation L_{tot} can be described by (1a) (Aubrecht et al., 2016; Incropera et al., 2006; FLIR, 2011), in its full form and in its simplified form (1b) close to the infrared camera (when atmospheric transmissivity τ is assumed to be 1):

$$L_{tot} = \tau\varepsilon_{obj}L_{obj} + \tau(1-\varepsilon_{obj})L_{bg} + (1-\tau)L_{air} \quad (1a)$$

$$L_{tot} = \varepsilon_{obj}L_{obj} + (1-\varepsilon_{obj})L_{bg} \quad (1b)$$

Infrared cameras calculate the apparent object temperature T_{ap} using operator-provided fixed values for ε_{obj}, L_{bg}, L_{air} and τ. When the objects (or parts of them) in an infrared image have different emissivities, the temperature of those pixels has to be adjusted. It is common practice to set the camera settings of ε and τ to 1.00 to simplify corrections in post-processing. Systematic camera error can be corrected by correlating the infrared measured temperature of a reference plate with a high emissivity ($\varepsilon_{emiss} \approx 1$; Fig. 1) with its independently measured temperature (Kim et al., 2018).

In ecological applications, the background thermal radiation L_{bg} has often been ignored due to the high emissivity of natural materials and relatively small contribution of L_{bg}. This is sufficiently accurate where only relative temperatures are required, but can lead to substantial errors in determining the actual temperature (Kim et al., 2016). L_{bg} could also be measured using independent sensors (Aubrecht et al., 2016), or using empirical correction equations (Kim et al., 2018). Measured air temperature and/or relative humidity have also been used to estimate L_{bg} (Birami et al., 2018). In the present study we added a low emissivity plate ($\varepsilon_{refl} \approx 0$, Fig. 1) with an integrated thermocouple, placed in the image frame. We were therefore able to measure L_{bg} near the sampled object in the same spectral range as the thermal measurements according to (2):

$$L_{bg} = \frac{L_{tot} - \varepsilon_{refl}L_{refl}}{1-\varepsilon_{refl}} \quad (2)$$

where L_{tot} is calculated using the Stefan–Boltzmann law ($L_{tot} = \varepsilon_{cam}\sigma T_{ap}^4$) from the apparent temperature T_{ap} reported by the infrared camera, using the Stefan-Boltzmann constant σ and the camera emissivity setting ε_{cam} (set to 1 to bypass internal camera corrections). ε_{refl} is the emissivity of the highly reflective plate and the thermal radiation emitted by it is $L_{refl} = \sigma T_{refl}^4$, where T_{refl} is the independently measured temperature of the reference plate (using a calibrated thermocouple). Employing a reflective reference plate with a $\varepsilon > 0.1$ is not recommended due to noise introduced from the plate's low reflectivity. Finally, the corrected object temperature can be calculated by applying the resulting L_{bg} in (1b).

2.3 Leaf and air temperature: Field measurements

Leaf temperatures were measured during the peak of summer drought, consecutively in different heights within the canopy in summer 2018 (3 m, 5 m, 7 m & 8.5 m) as well as in ~5 m (middle of the canopy) in a drought-exposed and experimentally irrigated plot in summers 2018 & 2019 (Measurement periods & location, cf. Table 1, map: Fig. S4.1). In the following text, leaf temperature will refer to the mean temperature of multiple needles on the same twig (as seen in Fig. 1b).

Thermal infrared measurements of T_{leaf}, T_{ref} and L_{bg} were done using an infrared camera (7.5-13μm; FLIR A320; FLIR Systems, Wilsonville, Oregon, United States) facing north installed on a mast, triggered automatically every 5 min (every 15 min before 2018-08-01) using a camera setting of $\varepsilon = 1.00$ and $\tau = 1.00$ due to the close distance of <65 cm between the infrared camera and the leaves (setup cf. Fig. 1). Other camera parameters were left to factory defaults ($T_{bg} = 20$°C, $T_{atm} = 20$°C), but are dropped due to $\varepsilon = 1$ and $\tau = 1$. At this distance, pixels were ~0.4 mm wide using a 15° lens, compared to a diameter of needle-leaves of ~0.8–1 mm, which allowed us to avoid mixed values between the background (sky, branches) and the leaves (leaves). The final temporal resolution was lower than 5 m in because the camera had to be restarted every few hours to circumvent crashes of the internal cam-

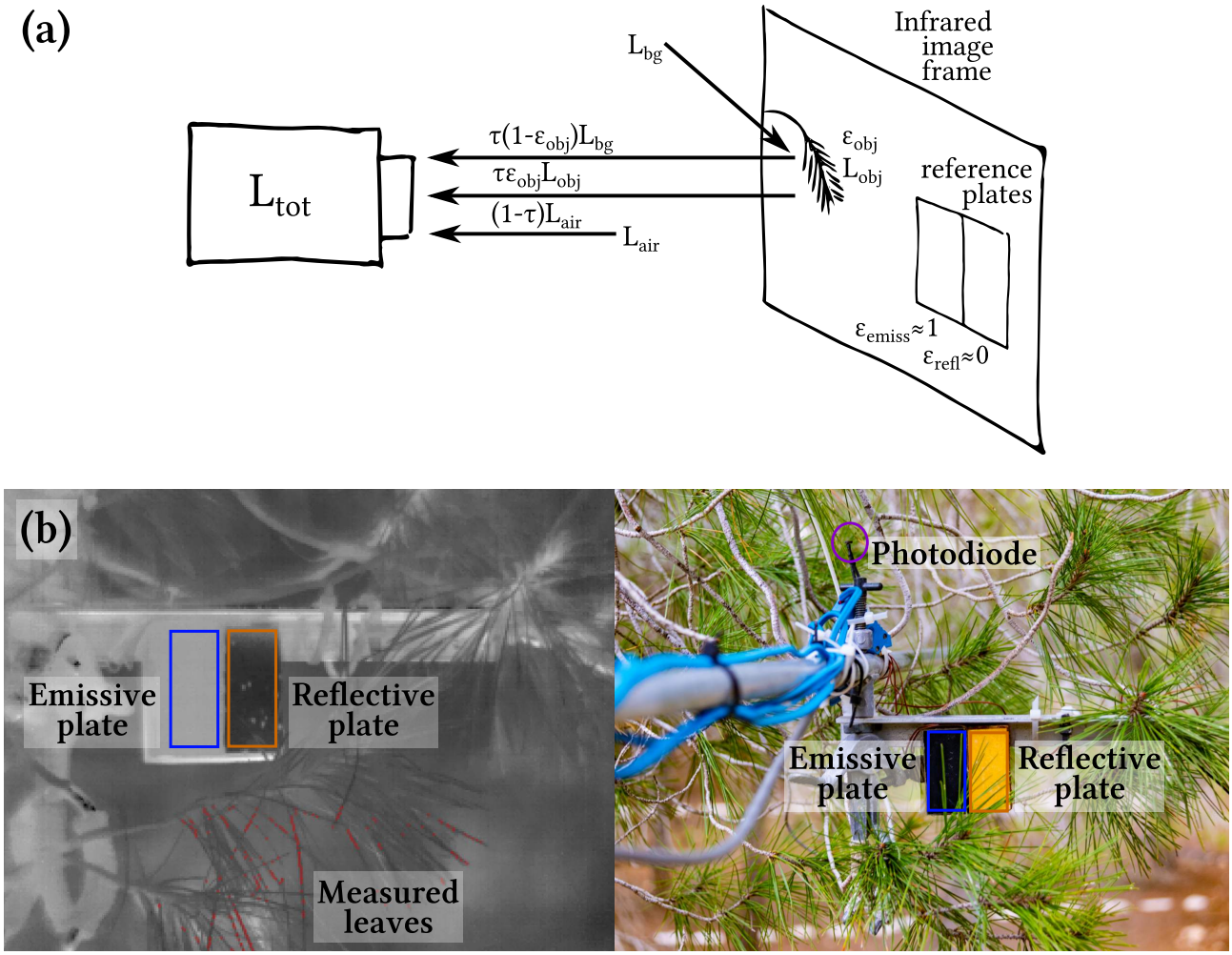

Fig. 1. (a) Illustration of the total radiation reaching an infrared camera (L_{tot}) and the relevant terms it receives, including a set of two reference plates with low (ε_{refl}) and high (ε_{emiss}) emissivities, respectively, in its field of view. Part of L_{tot} is emitted by the object (L_{obj}), by the air column (L_{air}) between it and the camera which attenuates it (τ), and part is a reflection of the background (L_{bg}) coming from surrounding objects and the sky. (b) Left side: Example infrared image where dark shades are colder; Right side: Setup of the infrared camera's picture frame. Red points show examples of pixels identified as leaves by automatic scripts. Polygons show the reference plates used for camera offset correction (emissive plate, blue) and background thermal radiation (reflective plate, orange) and a photodiode (purple) measured the incoming shortwave radiation.

era software, and measurements were averaged to half hours. An arm extending from the infrared camera held branches in a fixed position to minimise movement from wind and simplify image analysis. Systematic camera error, i.e. the offset from the real surface temperature, was corrected using measurements of a reference aluminium plate with a highly emissive coating (*Metal Velvet*™ coating; Acktar Ltd., Kiryat-Gat, Israel). For measurements of L_{bg}, we used a reference plate with a high reflectivity (Infragold coating; Labsphere Inc., North Sutton NH, USA; installed on 2018-09-06) alongside it. This reflective plate had a coarse surface, which allowed background radiation from a wide range of angles to be reflected into the thermal camera. Both plates had a thickness of 3 mm, and each contained a thin thermocouple installed in the middle of the plates, 0.5 mm from the coated surfaces in a tiny drilled hole filled with thermal grease. The plates were insulated by a piece of wood 2 cm thick on the back to prevent undesired heating from the air. Their hemispherical directional emissivities (at a right angle to the plates), as well as that of natural materials present in Yatir forest (leaves, branches, soil; $\varepsilon \approx 0.90$; Table 2) were measured in the lab using our special emissivity measurement instrument (Vishnevetsky et al. 2019) at an

uncertainty of <0.5 % for an emissivity >0.90 estimated based on the measurements summarised in Table 2. The total temperature measurement error of our system was 0.3 °C, as calculated from the combined errors of each sensor using the log derivative method (Fritschen and Gay, 2012).

A photodiode sensitive in the PAR range (400–700 nm; G1118, Hamamatsu Photonics K.K., Japan), calibrated against a commercial PAR sensor (PQS1, Kipp & Zonen, Delft, The Netherlands) and a shortwave full-range pyranometer with a 0–4000 nm range (CM21, Kipp & Zonen B.V., Delft, The Netherlands), was employed to measure incoming solar radiation near the leaves at 1 Hz. The light reaching this photodiode was assumed to be the same as in the entire field of view of the thermal camera.

At a distance of ~2 m from the camera mast, a 3D sonic anemometer installed on a second mast was used to measure local wind speed in 3D ($m\,s^{-1}$; Windmaster Pro, Gill Instruments, Lymington, United Kingdom). Data was logged on a field computer using a LabVIEW (National Instruments; Austin, Texas USA) software. For precise air temperature measurements, a calibrated fine T-type thermocouples were installed in Young radiation shields (Model 41003; R. M. Young Company, Traverse City MI, USA) in the same height as the anemometers. Calibration of all thermocouples was done in stirred water of a known uniform temperature to remove differences of individual thermocouple junctions, as well as against a precise air temperature thermistor in a radiation shield. The accuracy of the thermocouples was 0.1 °C, that of the FLIR A320 infrared camera was 50 mK at 30 °C (FLIR, 2011).

2.4 Data extraction & outlier removal

A matrix of raw infrared temperatures were extracted from the FLIR infrared images using a Python script developed based on an R script by Tattersall (2019). Different areas of interest were scanned in horizontal lines to identify needle leaves and reference plates. A peak detection algorithm contained in SciPy (Virtanen et al., 2020) was used on each line to create a mask of valid pixels of each category: (a) To identify needles, a peak prominence of a height of ⅓ of the total range of values in each line and a maximum width of 5 px was used; (b) to identify reference plates, the junction of values between the 'warm' emissive and the 'cold' reflective plate was identified by calculating the first discrete difference along the horizontal line of data points, areas with a fixed width of 20 px around that junction were selected and peaks in those areas were removed (e.g. for leaves in front of the plates). The median, mean and standard deviations of all leaf temperatures of a twig were calculated for all the pixels in each category of data (i.e. leaves and reference plates), but medians were used to reduce the effect of obvious outliers. The results of this script were compared to manual sampling of leaf temperatures ($R^2 > 0.99$, $P < .001$; Fig. S1.1), showing that the script accurately extracts needle temperatures. Then, half-hourly means and standard deviations were calculated from the median and standard deviations of leaf temperatures of each infrared image.

The systematic camera offset was calibrated for the entire dataset of ~28'000 measurements using the emissive plate's night-time temperature (to avoid external heating of the plate). The plate temperature was measured by the built-in thermocouple and the infrared camera ($T_{IR} = 2.51 + 0.93T_{tc}$, $R^2 = 0.99$, $P < .001$) for every captured IR image. Then, the background radiation L_{bg} was calculated from the reflective plate (eq. 2). Due to the heat capacity of aluminium, thermocouples inside the reference plates react more slowly to fast plate surface temperature fluctuations seen by the IR camera, resulting from airflow and sudden sun spots on the surface of the plate. Therefore, data points where the difference between infrared and thermocouple temperature exceeded ±2 °C (<1 % of all data) were removed. Before the installation of the reflective plate on 2018-09-06, the surface temperature of the emissive plate was used to calibrate the IR camera readings of the leaf surface temperatures using a linear correlation, which is estimated to introduce an additional mean error of 0.08 ± 0.07 °C (max. 0.48 °C) for leaves or 0.25 ± 0.19 °C (max. 1.20 °C) for branches.

Table 2. Mean hemispherical directional emissivity with number of samples (N) and standard deviation of multiple samples of different materials measured in the lab using our custom made system (Vishnevetsky et al., 2019). For an emissivity $\varepsilon > 0.90$, the uncertainty is ≤0.5% of the measured ε, $\varepsilon < 0.95$, the uncertainty is ≤0.4%, for $\varepsilon \leq 0.1$, the uncertainty is ~28.6%

Sample Materials	N	Emissivity	Std. Dev.
Branch bark	4	0.896	0.014
1st emissive Acktar coating; before 2018-09-06	1	0.984	
2nd emissive Acktar coating; after 2018-09-06	1	0.977	
Reflective Infragold coating	1	0.023	
Pine needles (dry)	3	0.933	0.010
Pine needles (fresh; 1-3 years old)	4	0.947	0.003
Topsoil (Yatir research site)	4	0.933	0.006

3 Results

Accurate measurement of leaf temperature: To achieve the accuracy required to assess the leaf temperature T_{leaf} and, in turn, leaf-to-air temperature differences $\Delta T_{leaf-air}$ in our field study site, a special measurement system was constructed and tested.

The results demonstrate the critical importance of measuring L_{bg} under field conditions due to its large fluctuations. The sensitivity of the temperature measurements to different levels of L_{bg} was estimated for the range encountered in a natural environment such as the Yatir forest (300–500 W m^{-2}), and could be >1.5 °C for needle leaves and >3.5 °C for branches (Fig. 2), depending on the object's surface temperature. Such effects clearly limit any attempt to accurately assess $\Delta T_{leaf-air}$ under field conditions. Using continuous background corrections and camera calibration (see Methods), an accuracy of 0.3 °C and a precision of 0.1 °C is estimated, and is therefore a critical factor in the assessment of $\Delta T_{leaf-air}$ (an extended technical analysis of the leaf temperature methodology is beyond the scope of this paper, and will be reported separately).

No effect of transpiration rates: $\Delta T_{leaf-air}$, measured using the high precision temperature measurement system, and transpiration Tr, measured using automated branch-scale gas exchange chambers, during the 2018-2019 study period are summarized in Figure 3. Transpiration reached maximum values of 0.204 ± 0.162 mmol m−2 s^{-1} and 10x higher values of 2.294 ± 0.873 mmol m−2 s^{-1} in the drought-exposed and irrigated plots, respectively.

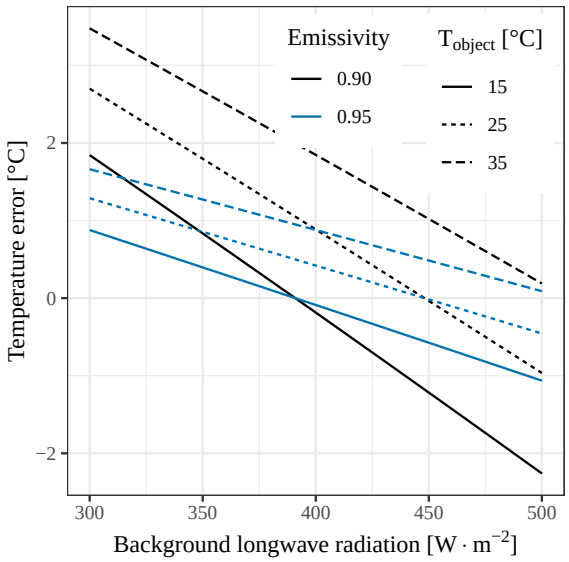

Fig. 2. Effect of object temperature (line type), emissivity (colour) and background thermal radiation on infrared temperature error [°C] in field conditions, using emissivity 0.95 (e.g. leaves) and 0.90 (e.g. branches), and background thermal radiation in field conditions ranging from 300–500 W m^{-2}, with three object temperatures ranging between 15–35 °C

The canopy air temperature in the two plots was similar and ranged between 18.16 ± 1.61 °C and 32.84 ± 2.12 °C on average from midnight to midday, respectively. Mean $\Delta T_{leaf-air}$ values ranged between 0.5 °C and 4.0 °C.

$\Delta T_{leaf-air}$ values showed a clear dependence on incoming solar radiation SWR (drought-exposed: $\Delta T_{leaf-air} = 1.92 + 0.002$SWR, $R^2 = 0.78$, $P < .001$; irrigated: $\Delta T_{leaf-air} = 0.85 + 0.003$SWR, $R^2 = 0.85$, $P < .001$). Note, however, that while the $\Delta T_{leaf-air}$ vs. SWR relationships could be well described by linear correlation, the data may also indicate an approach to a maximum

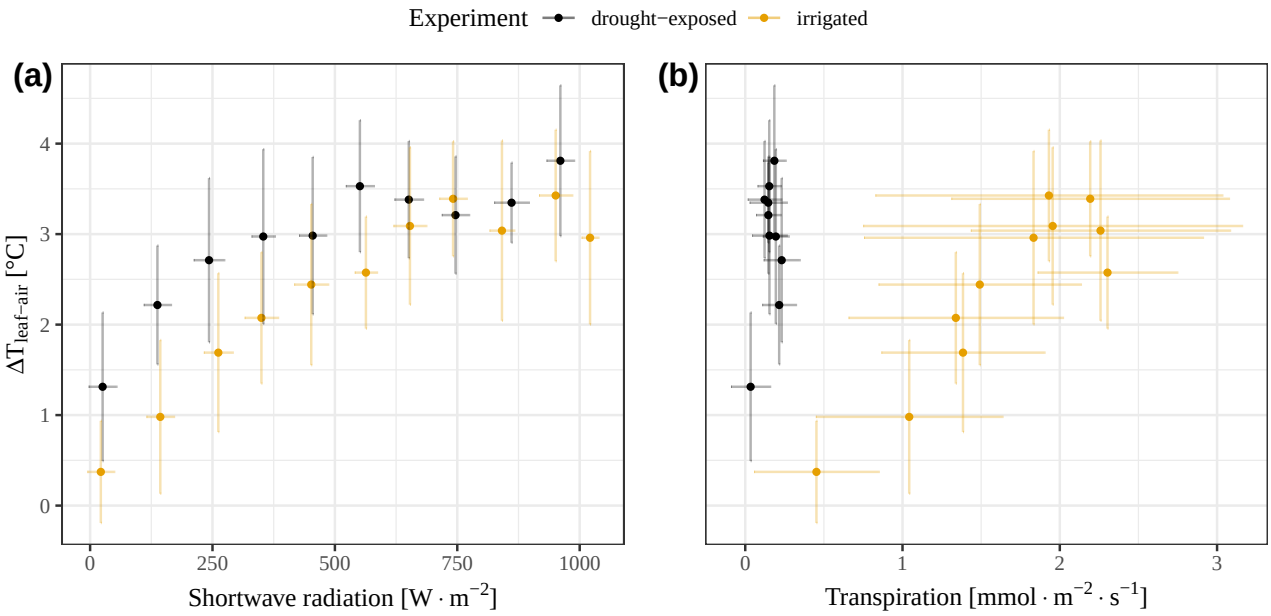

Fig. 3. Relationship between leaf-to-air temperature difference $\Delta T_{leaf-air}$ and (a) shortwave radiation and (b) transpiration in bins of 100 W m^{-2}, measured in summers 2018 & 2019 in irrigated (yellow) and drought-exposed trees (black). Bars represent standard deviations for each bin.

$\Delta T_{leaf-air}$ values in both treatments (Fig. 3a). Leaves of drought-exposed trees reached a maximum $\Delta T_{leaf-air} > 4.5$°C at 1000 W m^{-2}, while irrigated trees reached $\Delta T_{leaf-air}$ values of ~4 °C under similar conditions. Differences between both treatments were not significant (Fig. 3a), in spite of slightly higher average radiation exposure in the irrigation plot than in the drought-exposed plot due to natural variations in gaps in the canopy that influenced the extent of direct exposure to sunlight. The similarity in the $\Delta T_{leaf-air}$ versus SWR in the two treatments was also supported by later measurements using a portable leaf scale system (Fig. S3.1).

A different correlation between Tr and $\Delta T_{leaf-air}$ was exhibited in the two treatments (Fig. 3b; drought-exposed leaves: $\Delta T_{leaf-air} = 2.14 + 5.091\text{Tr}$, $R^2 = 0.15$, $P = 0.268$; and irrigated: $\Delta T_{leaf-air} = -0.25 + 1.584\text{Tr}$, $R^2 = 0.83$, $P < .001$). These correlations indicated, first, that evaporative cooling in itself does not prevent leaf heating (i.e., $\Delta T_{leaf-air}$ increased in spite of large increase in Tr; Fig. 3b), and second, that the same maximum $\Delta T_{leaf-air}$ value was observed in the two treatments in spite of the 10x difference in Tr values.

Factors affecting leaf to air temperature differences: $\Delta T_{leaf-air}$ and the factors that can influence it were examined in more detail in the drought-exposed, i.e. control, plot and are summarized in Figure 4. Shortwave radiation measurements (SWR) highlight the differences in shading in the different heights (Fig. 4c), which was associated with the orientation of the mast and the complex canopy structure in this field study. Therefore, the infrared camera measured more exposed leaves of the canopy skin in 7 m, where SWR levels were similar to the ones above canopy (up to ~1000 W m^{-2}). In 3, 5 & 8.5 m, canopy shading reduced mean SWR input (max. 550 W m^{-2}).

Leaf-to-air temperature differences ($\Delta T_{leaf-air}$, Fig. 4a, c) did not simply follow variations in SWR. For example, $\Delta T_{leaf-air}$ remained below 4 °C, and on average below 3.5 °C in 3 m and below 2.5 °C in 8.5 m in spite of similar levels of SWR (<550 W m^{-2}). Variations in T_{leaf} mostly paralleled air temperature T_{air}, but remained above it at all times (Fig. 4d). However, after 9:00 in 5 m and 7 m, the increase in T_{leaf} slowed down below the rate of increase of T_{air} (Fig. 4b, d), leading to a stabilisation or even decrease of $\Delta T_{leaf-air}$ even though SWR, T_{leaf} and T_{air} were still rising. Against our expectations, $\Delta T_{leaf-air}$ was highest at the bottom of the canopy (3 m agl) where it in-

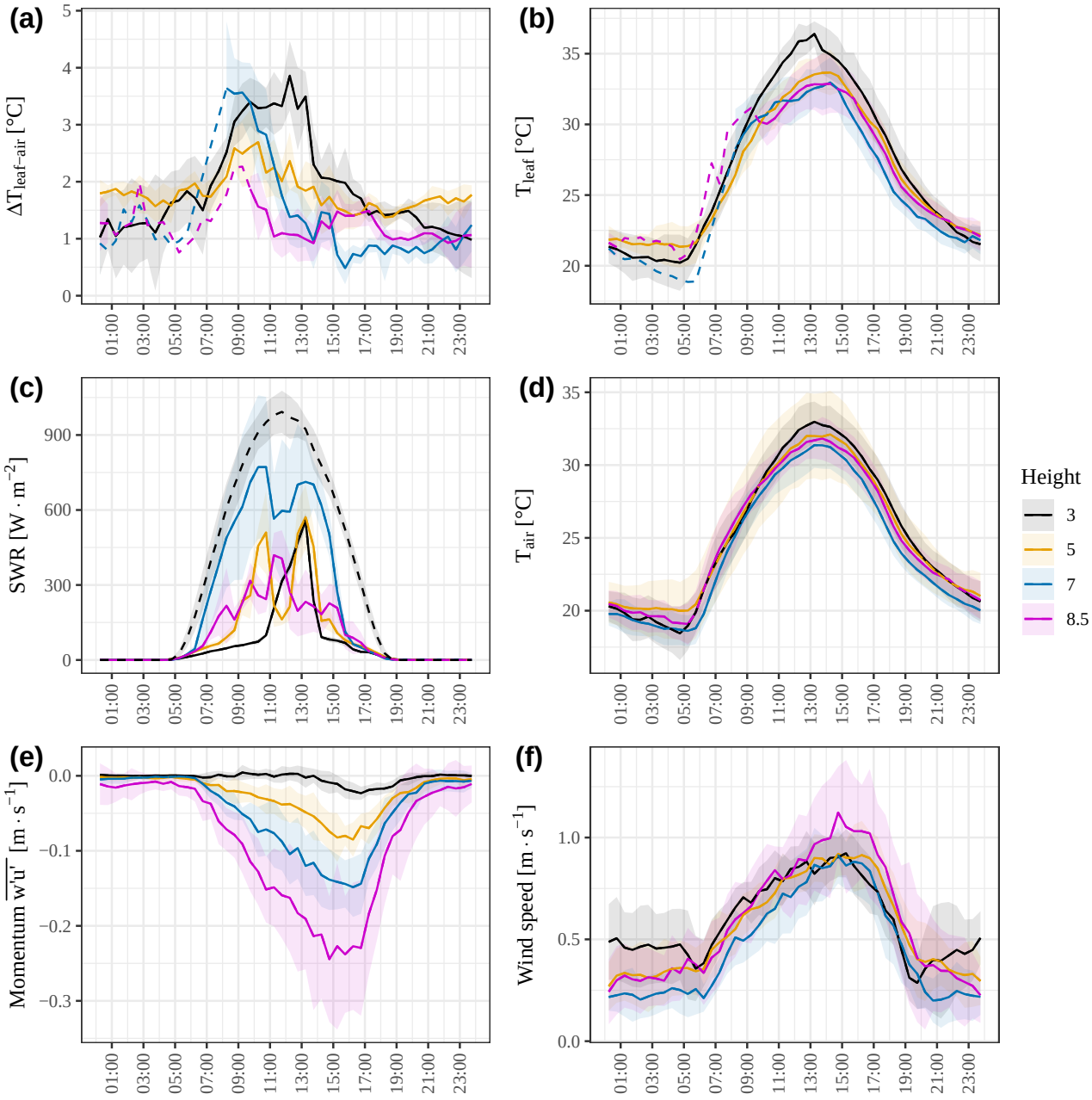

Fig. 4. Diurnals of half-hourly means over 2 weeks in the drought-exposed plot of (a) leaf-to-air temperature difference $\Delta T_{leaf-air}$ [°C], (b) leaf temperature T_{leaf} [°C], (c) incoming shortwave radiation SWR [W m^{-2}] with above-canopy SWR (dashed black), (d) air temperature T_{air} [°C], (e) mean half-hourly momentum of wind $\overline{w'u'}$ [m s^{-1}], (f) mean half-hourly wind speed u [m s^{-1}]. Colours represent different heights in the canopy (i.e. 3, 5, 7 & 8.5 m agl), solid lines depict times more than 3 available observations and shade is standard deviation, dashed lines have 1-2 observations (due to repeated camera failure).

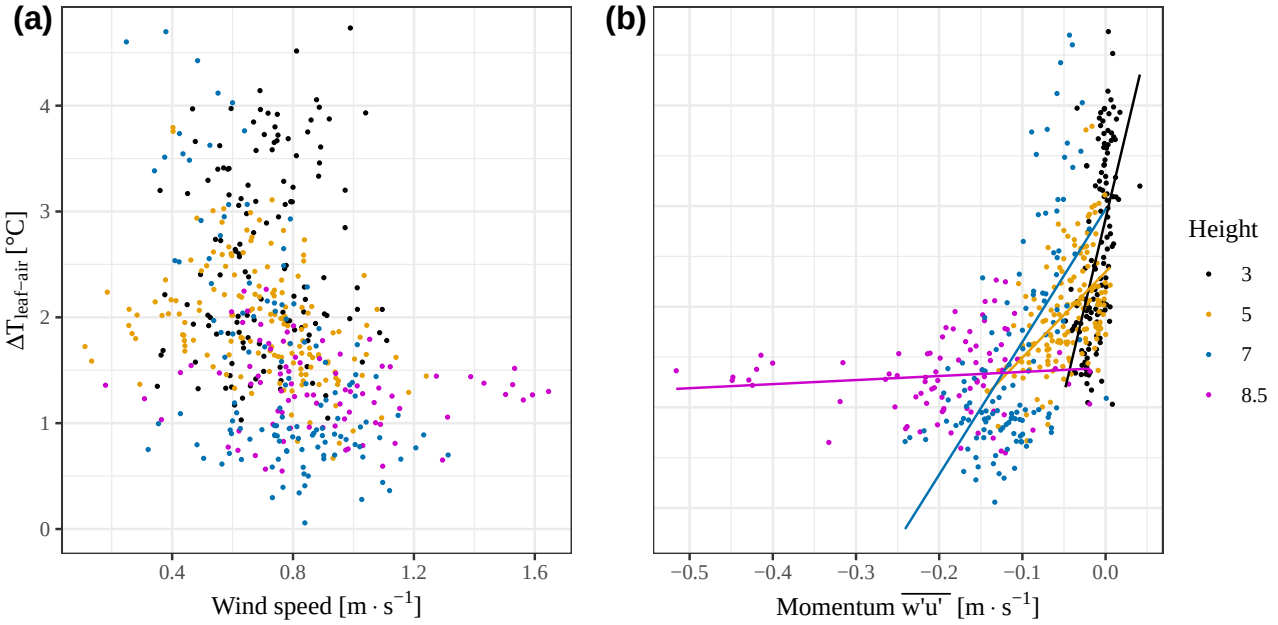

Fig. 5. Half-hourly means of leaf-to-air temperature difference $\Delta T_{leaf-air}$ [°C] with (a) mean wind speed u [m s^{-1}], (b) momentum of wind used to describe turbulence $\overline{w'u'}$ [m s^{-1}]. Colours represent different heights in the canopy (i.e. 3, 5, 7 & 8.5 m agl), lines are correlations between the variables

creased by 2.5 °C following sunrise, in spite of low SWR (<100 W m^{-2}). Furthermore, the independence of variations in T_{leaf} from those in SWR was especially clear in this canopy layer (3 m), where the stabilisation of $\Delta T_{leaf-air}$ at ~3.5 °C (9:00-13:00) occurred before the peak of solar radiation (13:00-14:00).

Mean half-hourly wind speed u was not significantly different between different heights (Fig. 4f), but turbulence did differ significantly, resulting from the interactions of wind speed and the canopy structure. For instance, turbulence was highest at the top of the canopy (-0.25 m s^{-1}, indicated by the mean half-hourly momentum of wind $\overline{w'u'}$; Fig. 4e). In 3 m, turbulence was nearly negligible (Momentum: $\overline{w'u'} > -0.01$ m s^{-1}) until ~13:00 (min. -0.048 m s^{-1}), but $\Delta T_{leaf-air}$ started to decrease as turbulence started to increase (negative values). In summary, our results do not show a direct dependence of $\Delta T_{leaf-air}$ on SWR and wind speed but rather on T_{air} and turbulence.

Mean wind speed u and turbulence (described using $\overline{w'u'}$), measured in 2 m distance of the leaves, show no correlation of u with $\Delta T_{leaf-air}$ (Fig. 5a), although it is typically associated with the leaf boundary layer and therefore wind cooling. However, $\Delta T_{leaf-air}$ was correlated with $\overline{w'u'}$ (3 m: $R^2 = 0.33$, $P < .001$; 5 m: $R^2 = 0.27$, $P < .001$; 7 m: $R^2 = 0.37$, $P < .001$; 8.5 m: $R^2 = 0.01$, $P = 0.35$). The onset of turbulence rapidly reduced $\Delta T_{leaf-air}$, and with a higher level of turbulence ($\overline{w'u'} < -0.15$ m s^{-1}), a minimum $\Delta T_{leaf-air}$ is maintained, i.e. ~1 °C inside the canopy or close to 0.5 °C at the canopy skin (7 m agl). Thus these result indicate the importance of air cooling only through the interactions of wind and canopy structure via turbulence.

4 Discussion

Key elements for accurate leaf temperature measurements: Accurate measurements of leaf temperature are crucial to understand many biochemical and biogeophysical processes, but are challenging, particularly under field conditions. A number of recent studies have focussed on using thermal infrared cameras (Still et al., 2019 and references therein), but those require corrections that are difficult to make, such as for the emissivity of the measured materials and for the background radiation, which is subject to large fluctuations in natural environments (Still et al.,

2019; Aubrecht et al., 2016), as well as systematic camera drift.

The results of this study identify several critical factors that limit infrared-based temperature measurements and demonstrate ways to overcome these limitations to obtain the precision required for the study of leaf and $\Delta T_{leaf-air}$ under field conditions. First, while direct measurement of emissivity is challenging, lab-scale high precision systems can be constructed and used to identify variations in ε of plant material (Vishnevetsky et al., 2019). Second, we show that significant variations in background thermal radiation under field conditions can lead to inaccuracies in the order of 3.5 °C in surface temperature (depending on the environment; Fig. 2). This could be overcome by using a highly reflective reference plate that captures the background longwave radiation. Third, infrared temperature measurements are restricted to the accuracy of the camera, in the range of 1–2 °C (Kim et al., 2016, 2018). This could be overcome by using a highly emissive plate with negligible effects of the background radiation to correct for systematic thermal camera offset. The temperature of both reference plates can be measured continuously using accurately calibrated thermocouples. Note that using a single highly emissive reference plate for continuous calibration seems to be insufficient to reduce measurement errors below ~1 °C (Aubrecht et al., 2016). In addition to these factors, the distance from the target, allowing for non-contact single needle-leaf observations at reasonably close proximity has to be chosen to obtain pixel size smaller than the leaf dimension (<1 mm diameter in the present study) to avoid signal contamination (e.g., from sky, soil and branches). Our results show that using the steps noted above, temperature measurements with precision of 0.1 °C, and accuracy of 0.3 °C, can be achieved on a routine basis even for small-dimension needle leaves under field conditions. These technical results were a prerequisite for this study, and on which the results discussed below are based (more technical details of the leaf temperature measurement approach will be published separately).

Non-evaporative vs. evaporative cooling: It is commonly assumed that evaporative cooling through transpiration Tr is the most effective heat dissipation mechanism (Wulfmeyer et al., 2014) and is key to optimize leaf temperature for the leaf biochemical processes (Dusenge et al., 2019). Evaporative cooling can result in a temperature reduction of up to 9 °C in broadleaf species (Urban et al., 2017). Furthermore, leaf temperature and $\Delta T_{leaf-air}$ provide an indicator of evaporative cooling, where warmer leaves indicate stomatal closure, more stress, and reduced gas exchange (e.g., Leuzinger and Körner, 2007; Kim et al., 2018). Evaporative cooling can also reflect the effects of other interacting factors that influence stomatal conductance, such as VPD (Kimball and Bernacchi, 2006), or rising CO_2 levels (Urban et al., 2017; Kimball and Bernacchi, 2006; Leakey et al., 2006; Long et al., 2006). Similarly, the effect of climate driven rise in temperatures on leaf assimilation and water loss will depend on the effects of concurrent changes in factors such as VPD in atmospheric CO_2 on leaf conductance, evaporation and, ultimately, its temperature (Dusenge et al., 2019; Kirschbaum and McMillan, 2018).

Our results indicated deviations from the common $\Delta T_{leaf-air}$ dependency on transpiration and stomatal conductance, as reflected in the similar $\Delta T_{leaf-air}$ in leaves with an order of magnitude difference in leaf transpiration. As discussed below, this can be achieved by changes in the leaf sensible heat flux, that must reflect changes in the leaf resistance to heat transport, which could be associated, in turn, with the small anatomical, structural and spectral differences observed between the leaves of drought-exposed and irrigated trees.

We observed that transpiration at the highest radiation bin translates to a latent heat LE of ~8 W m^{-2} in the drought-exposed, and 10x times higher value of ~85 W m^{-2} in the irrigated trees. This reflects a major change in the leaf energy budget, which can be described as:

$$R_n = H + LE + G + B \quad (3)$$

where R_n is the net radiation, and G and B are net physical heat storage and energy taken up by biochemical reactions, which are typically considered negligible (Schymanski et al., 2013). Preliminary estimates of R_n in the two study plots indicated similar mean values of 334±11 (n=10) and 330±14 W m^{-2} (n=24) in the drought-exposed

and irrigated plots, respectively, for the aforementioned radiation bin (a more detailed analysis of the leaf radiation budget, beyond the scope of this study, will be published separately, but its effect on the mean R_n values is small). With measured values of R_n and LE, and negligible effects of G and B in (3), the leaf energy budget can only be adjusted via the sensible heat flux H. This indicates a large difference in H between the control (~326 W m^{-2}) and irrigated (~245 W m^{-2}) trees. The sensible heat flux can, in turn, be described by:

$$H = \rho c_p \frac{\Delta T_{leaf-air}}{r_H} \tag{4}$$

where c_p and ρ are the heat capacity and density of air surrounding the leaves, and r_H is the leaf resistance to heat transfer (where 'leaf' denotes multiple needles on a small twig; see Methods). Note that a simple sensitivity test indicates that a difference of 15 mmol mol^{-1} in air moisture or 5 °C in air temperature (when ambient T_{air} is ~30°C) near leaves would produce a change in H of ~2.5–10 W m^{-2} due to changes c_p and ρ. Assuming, for a first approximation, that differences in air c_p and ρ between the nearby plots were negligible, the difference in H derived above for the control and irrigated leaves, requires a proportional change in r_H, (i.e. 326/245 = 1.33). In other words, under similar R_n conditions, the efficient non-evaporative cooling observed in the control leaves must involve >30 % decrease in r_H.

Factors contributing to change in resistance to heat exchange at the leaf scale: Adaptation in plants has optimised canopy structures and leaf shapes, among other things, for convective cooling (Smith, 1978). This can happen through an enhanced air flow and reduced r_H, while concurrently minimizing its negative effects on evaporative water loss (Schymanski and Or, 2016; Grace and Wilson, 1976). Leaf and branch resistance to heat dissipation and the production of H is affected by factors that mainly modify the leaf boundary layer size or the flow of air surrounding the leaves. Often, r_H has been parametrised using air flow variables measured above the canopy, i.e. wind speed u (Jones, 2004; Kool et al., 2016; Kustas and Norman, 1999; Verma, 1989) and shear velocity u_* (Baldocchi and Ma, 2013; Liu et al., 2007), which indicates an increased local turbulence. Additionally, there are numerous reports of leaf anatomical, structural, and surface effects on convective cooling. For example, Leigh et al. (2012, 2017) demonstrate clear relationships between $\Delta T_{leaf-air}$ and leaf shape and thickness, resulting in a $\Delta T_{leaf-air}$ range of 2–10 °C. These studies also indicate the trade-offs between the leaf heat capacity that helps to deal with fast intense radiation exposure fluctuations, and the leaf size required to reduce r_H. Leaf surface structures such as veins or hairs also affect roughness and therefore the generation of turbulence, which can improve convective cooling, as does leaf orientation relative to the wind direction (Schuepp, 1993; Grace and Wilson, 1976; Grace et al., 1980). Needle-leaves, such as used in this study, may be a good example of low resistance leaves, based on their shape and surface to volume ratio, which all minimise the size of the boundary layer while maintaining sufficient leaf heat capacity.

Within the same species and at the same site, large changes in leaf and branch r_H are more difficult to explain. But as argued above, the drought-exposed and irrigated trees must also exhibit some adjustments that produce large differences in r_H between them. Indeed, preliminary observations indicated some changes in leaf/twig characteristics, resulting from the summer supplement irrigation. As a result, in the drought-exposed plot, needle-leaves were significantly shorter (and slightly but not significantly thicker), had a reduced clumpiness (needle density per twig), and lower chlorophyll content (Table S5.1, Figs. S5.1, S5.2 and S6.1). Shorter leaves and reduced clumpiness are consistent with reduced r_H in different plant species, as a result of simple vs. complex leaves that allow for more efficient air flow (Leigh et al., 2017). Early studies already noted the importance of leaf dimensions in estimating the leaf boundary layer resistance to heat transfer r_H (e.g., Monteith, 1973), and Balding and Cunningham (1976) developed an empirical model that relates r_H to leaf dimensions (length l, and width w), and wind speed (v; $r_H = k\frac{l^x w^y}{v^z}$). Using such relationships and their empirically derived power terms indicate that the observed change in leaf length in our study (Table S5.1) is sufficient to reduce r_H by about 30 %. A similar effect can be associated with doubling of the local wind speed, which can be associated with the reduced clumpi-

ness (Table S5.1; Fig. S6.1), or some combination of these and other yet unidentified effects. The reduced needle density on twigs could also increase the twig roughness, and enhance turbulence (see next section), while the reduced pigment concentration under dry conditions (Table S5.1) could help in reducing leaf heating and increased reflectivity.

Clearly, the detailed estimation of changes in leaf resistance to heat dissipation requires, and justifies, further research. However, the available information provides strong supporting evidence to the hypothesis that significant changes in r_H within the same species and location are possible under different soil moisture conditions. These conclusions, in turn, support the idea that efficient non-evaporative cooling can be developed in pine trees under dry conditions, based on a reduced r_H and the generation of a large H. This results in a low $\Delta T_{leaf-air}$ similar to that of high transpiration leaves that rely on a combination of higher r_H and higher Tr to maintain a low $\Delta T_{leaf-air}$.

Linking leaf temperature to canopy structure and turbulence: While the importance of surface roughness and structure is seldom considered at the leaf scale, such effects have been clearly demonstrated at the ecosystem scale (Zhang et al., 2020; Rotenberg and Yakir, 2010, 2011). Sparse canopies, such as in our open-canopy forest, allow for the penetration of wind and efficient heat exchange through a higher roughness and reduced canopy scale r_H (Banerjee et al., 2017; Eder et al., 2015). In our measurement, this could reduce leaf temperatures to within 3.5 °C of the air. The vegetation type (conifers vs broadleaves) and the observation point (top vs. within canopy) can also contribute to the range of observed canopy-air temperature differences of −2 to 10 °C (Table S7.1).

Our measurements of needle-leaf temperature in different heights of the canopy with distinct shading regimes showed that higher mean SWR does not always translate to a high $\Delta T_{leaf-air}$. Instead, T_{leaf} generally paralleled T_{air} during most of the day (Fig. 4b,d). In some periods, such as during the 9:00 to 14:00 period, the increase of T_{leaf} fell below that of T_{air}, hence $\Delta T_{leaf-air}$ no longer increased. Furthermore, at the bottom of the canopy (3 m agl) where SWR remained below 550 W m^{-2}, $\Delta T_{leaf-air}$ reached 3.5 °C throughout the day, while in the exposed upper part of the canopy (7 m), $\Delta T_{leaf-air}$ remained around 2 °C in spite of high SWR of ~1000 W m^{-2}. This suggests that T_{air} is a more dominant driver of T_{leaf}, while SWR can be an indirect driver affecting T_{air} on an ecosystem scale. In our example of a low density forest, SWR heats up a significant fraction of exposed ground, resulting in the production of large thermal radiation and sensible heat flux that heat up the bottom of the canopy, in what was previously described as a 'canopy greenhouse' effect (Rotenberg and Yakir, 2011).

In addition to the unexpectedly ambiguous effects of SWR on leaf temperature, the effects of wind speed and, in turn, turbulence can be at least as important. At the study site, wind speed was not directly correlated with $\Delta T_{leaf-air}$ (Fig. 4), but the decrease of $\Delta T_{leaf-air}$ with height coincided with the onset of turbulence, described using the momentum of wind $\overline{w'u'}$ (Fig. 4a,e). Indeed, with $\overline{w'u'} > -0.2$ m s^{-1}, $\Delta T_{leaf-air}$ remained nearly constant. This explains the suppression of the expected high $\Delta T_{leaf-air}$ at around 2 °C at the top of the canopy (8.5 m), while $\Delta T_{leaf-air}$ reached ~4 °C at the bottom (3 m) where turbulence was low ($\overline{w'u'} > -0.05$ m s^{-1}). Note that across canopy layers, the aerodynamic resistance to heat transfer is additionally a function of $\Delta T_{canopy-air}$ at that scale. The observed effects of turbulence on $\Delta T_{leaf-air}$ (Fig. 5) must, therefore, influence also this within-canopy resistance to heat transfer.

These results provide an opportunity to explain the $\Delta T_{leaf-air}$ distribution across the canopy, particularly in our xeric forest (Fig. 6). As noted above, at the bottom of the canopy (3 m agl) the combination of the lowest turbulence and the heating from the ground results in the highest $\Delta T_{leaf-air}$ of 3.5 °C (Fig. 4). Conversely, in exposed leaves in 7 m (mean half-hourly solar radiation: ~1000 W m^{-2}), $\Delta T_{leaf-air}$ rapidly drops from ~3.5 to 1 °C by noon due to the high turbulence, increasing due to the interaction of the regional sea breeze with the roughness of the forest canopyand in spite of a high air temperature. Finally, $\Delta T_{leaf-air}$ of shaded leaves below the top of the canopy (8.5 m) was suppressed all day long and remained below 2 °C. These leaves seem to benefit from the combined effects of the shading,

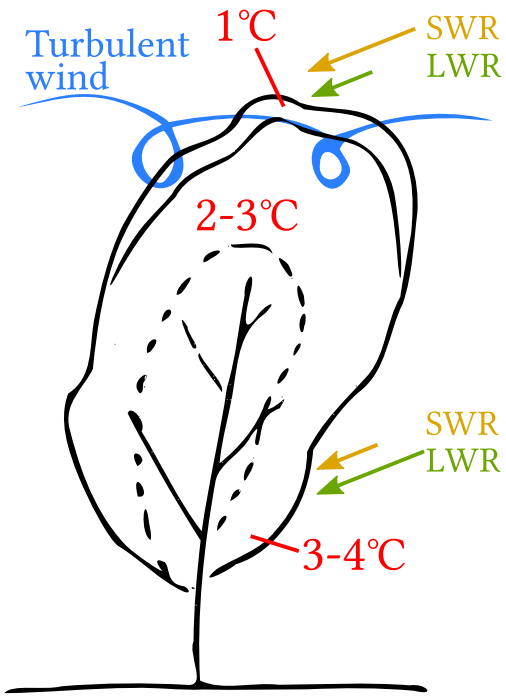

Fig. 6. Conceptual diagram of the distribution of $\Delta T_{leaf-air}$ within the canopy structure, indicating the observed $\Delta T_{leaf-air}$ values in the different layers in this study, in relations to the radiation input of short wave and long wave radiations (SWR and LWR) from the surroundings as well as air cooling effects through turbulent wind.

the low incoming LWR from the cold atmosphere (as compared to the soil in the lower canopy), and maximal turbulence, which increases air-cooling through an increased turbulent air flow.

The apparent contrast between the near-top and bottom of the canopy demonstrates the importance of turbulence within the canopy in controlling $\Delta T_{leaf-air}$, which relies on the reduced leaf-scale r_H resulting from anatomical and biophysical adjustments. Additionally, the canopy density and structure in this xeric ecosystem seems to maximize the canopy-scale, turbulence-based, air-cooling of leaves. Note that this efficient air cooling through turbulent wind penetration into the canopy also has implications for the development of the large sensible heat flux out of the forest canopy, described by Banerjee et al. (2017) as a cause of the generation of the so called canopy 'convector effect'.

Acknowledgements

The authors are grateful to Tamir Dingjan for his help with needle-leaf identification in Python and for proof-reading, Huanhuan Wang for chlorophyll measurements, Irina Vishnevetsky for emissivity measurements of different materials and Revital Weic for her manual sampling of needle-leaf temperature.

This study was supported by by JNF-KKL (10-10-920-19), the German Research Foundation (DFG) as part of the project *Climate feedbacks and benefits of semiarid forests* (CliFF) and a research grant from the *Yotam project* and the *Weizmann Institute Sustainability and Energy Research Initiative*. The long-term operation of the Yatir Forest Research Field Site is supported by the *Cathy Wills and Robert Lewis Program in Environmental Science*.

Author contributions

The study was conceived by JM,ER and DY; JM developed the IR system,and carried out the measurements with the help of IO and FT; JM analysed the data under the guidance of ER and DY; JM,ER and DY contributed to the writing.

Code and data availability

The data that support the findings of this study are available from the corresponding author upon reasonable request. Software scripts developed for the analysis are openly available as follows:

- Script to analyse gas exchange chamber flux data: 'Branch-chamber-fluxes' at https://doi.org/10.5281/zenodo.4284487, reference (Muller and Oz, 2020)
- Script to automatically trigger an infrared camera through a LAN interface: 'FLIR-A320-control' at https://doi.org/10.5281/zenodo.4088156, reference (Muller, 2020)
- Python script to extract raw temperature data from FLIR infrared images: 'IR-

data-extraction' at https://doi.org/10.5281/zenodo.4104314, reference (Muller and Segev, 2020)

- Script to detect pine needles and reference plates in infrared images: 'Pine-needle-thermal-detection' at https://doi.org/10.5281/zenodo.4284621, reference (Muller and Dingjan, 2020)

References

Allen, C. D., Macalady, A. K., Chenchouni, H., Bachelet, D., McDowell, N., Vennetier, M., Kitzberger, T., Rigling, A., Breshears, D. D., Hogg, E. H. T., Gonzalez, P., Fensham, R., Zhang, Z., Castro, J., Demidova, N., Lim, J.-H., Allard, G., Running, S. W., Semerci, A., and Cobb, N. A global overview of drought and heat-induced tree mortality reveals emerging climate change risks for forests. *Forest Ecology and Management*, 259(4):660–684, February 2010. doi:10.1016/j.foreco.2009.09.001.

Allen, C. D., Breshears, D. D., and McDowell, N. On underestimation of global vulnerability to tree mortality and forest die-off from hotter drought in the Anthropocene. *Ecosphere*, 6(8): art129, 2015. doi:10.1890/ES15-00203.1.

Aubrecht, D. M., Helliker, B. R., Goulden, M. L., Roberts, D. A., Still, C. J., and Richardson, A. D. Continuous, long-term, high-frequency thermal imaging of vegetation: Uncertainties and recommended best practices. *Agricultural and Forest Meteorology*, 228–229:315–326, November 2016. doi:10.1016/j.agrformet.2016.07.017.

Balding, F. R. and Cunningham, G. L. A comparison of heat transfer characteristics of simple and pinnate leaf models. *Botanical Gazette*, 137 (1):65–74, 1976.

Baldocchi, D. and Ma, S. How will land use affect air temperature in the surface boundary layer? Lessons learned from a comparative study on the energy balance of an oak savanna and annual grassland in California, USA. *Tellus B: Chemical and Physical Meteorology*, 65(1):19994, December 2013. doi:10.3402/tellusb.v65i0.19994.

Baldocchi, D. and Penuelas, J. The physics and ecology of mining carbon dioxide from the atmosphere by ecosystems. *Global Change Biology*, 25(4):1191–1197, 2019. doi:10.1111/gcb.14559.

Banerjee, T., De Roo, F., and Mauder, M. Explaining the convector effect in canopy turbulence by means of large-eddy simulation. *Hydrology and Earth System Sciences (Online)*, 21 (LA-UR-17-22651), 2017.

Birami, B., Gattmann, M., Heyer, A. G., Grote, R., Arneth, A., and Ruehr, N. K. Heat Waves Alter Carbon Allocation and Increase Mortality of Aleppo Pine Under Dry Conditions. *Frontiers in Forests and Global Change*, 1, 2018. doi:10.3389/ffgc.2018.00008.

Bonan, G. B. Forests and Climate Change: Forcings, Feedbacks, and the Climate Benefits of Forests. *Science*, 320(5882):1444–1449, June 2008. doi:10.1126/science.1155121.

Drake, J. E., Tjoelker, M. G., V\a arhammar, A., Medlyn, B. E., Reich, P. B., Leigh, A., Pfautsch, S., Blackman, C. J., López, R., and Aspinwall, M. J. Trees tolerate an extreme heatwave via sustained transpirational cooling and increased leaf thermal tolerance. *Global change biology*, 2018.

Dusenge, M. E., Duarte, A. G., and Way, D. A. Plant carbon metabolism and climate change: elevated CO 2 and temperature impacts on photosynthesis, photorespiration and respiration. *New Phytologist*, 221(1):32–49, 2019.

Eder, F., De Roo, F., Rotenberg, E., Yakir, D., Schmid, H. P., and Mauder, M. Secondary circulations at a solitary forest surrounded by semi-arid shrubland and their impact on eddy-covariance measurements. *Agricultural and Forest Meteorology*, 211:115–127, 2015.

FLIR. FLIR A3xx series - User's manual. Publ. No. T559498 Rev. a547, FLIR, July 2011.

Fritschen, L. J. and Gay, L. W. *Environmental Instrumentation*. Springer Science & Business Media, December 2012. ISBN 978-1-4612-6205-3.

Geller, G. and Smith, W. Influence of leaf size, orientation, and arrangement on temperature

and transpiration in three high-elevation, large-leafed herbs. *Oecologia*, 53(2):227–234, 1982. doi:10.1007/BF00545668.

Grace, J. and Wilson, J. The Boundary Layer over a Populus Leaf. *Journal of Experimental Botany*, 27(2):231–241, April 1976. doi:10.1093/jxb/27.2.231.

Grace, J., Fasehun, F. E., and Dixon, M. Boundary layer conductance of the leaves of some tropical timber trees. *Plant, Cell & Environment*, 3(6):443–450, 1980. doi:https://doi.org/10.1111/1365-3040.ep11586917.

Idso, S. B., Jackson, R. D., Ehrler, W. L., and Mitchell, S. T. A Method for Determination of Infrared Emittance of Leaves. *Ecology*, 50(5): 899–902, 1969. doi:10.2307/1933705.

Incropera, F. P., DeWitt, D. P., Bergman, T. L., and Lavine, A. S. *Fundamentals of Heat and Mass Transfer*. John Wiley & Sons, Hoboken, NJ, 6th edition edition, March 2006. ISBN 978-0-471-45728-2.

Jones, H. G. Application of Thermal Imaging and Infrared Sensing in Plant Physiology and Ecophysiology. In *Advances in Botanical Research*, volume 41 of *Incorporating Advances in Plant Pathology*, pages 107–163. Academic Press, January 2004. doi:10.1016/S0065-2296(04)41003-9.

Kim, Y., Still, C. J., Hanson, C. V., Kwon, H., Greer, B. T., and Law, B. E. Canopy skin temperature variations in relation to climate, soil temperature, and carbon flux at a ponderosa pine forest in central Oregon. *Agricultural and Forest Meteorology*, 226–227:161–173, October 2016. doi:10.1016/j.agrformet.2016.06.001.

Kim, Y., Still, C. J., Roberts, D. A., and Goulden, M. L. Thermal infrared imaging of conifer leaf temperatures: Comparison to thermocouple measurements and assessment of environmental influences. *Agricultural and Forest Meteorology*, 248:361–371, January 2018. doi:10.1016/j.agrformet.2017.10.010.

Kimball, B. A. and Bernacchi, C. J. Evapotranspiration, Canopy Temperature, and Plant Water Relations. In Nösberger, J., Long, S. P., Norby, R. J., Stitt, M., Hendrey, G. R., and Blum, H., editors, *Managed Ecosystems and CO2: Case Studies, Processes, and Perspectives*, Ecological Studies, pages 311–324. Springer, Berlin, Heidelberg, 2006. ISBN 978-3-540-31237-6. doi:10.1007/3-540-31237-4_17.

Kirschbaum, M. U. F. and McMillan, A. M. S. Warming and Elevated CO2 Have Opposing Influences on Transpiration. Which is more Important? *Current Forestry Reports*, 4(2):51–71, June 2018. doi:10.1007/s40725-018-0073-8.

Kool, D., Kustas, W. P., Ben-Gal, A., Lazarovitch, N., Heitman, J. L., Sauer, T. J., and Agam, N. Energy and evapotranspiration partitioning in a desert vineyard. *Agricultural and Forest Meteorology*, 218:277–287, March 2016. doi:10.1016/j.agrformet.2016.01.002.

Kustas, W. P. and Norman, J. M. Evaluation of soil and vegetation heat flux predictions using a simple two-source model with radiometric temperatures for partial canopy cover. *Agricultural and Forest Meteorology*, 94(1):13–29, April 1999. doi:10.1016/S0168-1923(99)00005-2.

Lapidot, O., Ignat, T., Rud, R., Rog, I., Alchanatis, V., and Klein, T. Use of thermal imaging to detect evaporative cooling in coniferous and broadleaved tree species of the Mediterranean maquis. *Agricultural and Forest Meteorology*, 271:285–294, June 2019. doi:10.1016/j.agrformet.2019.02.014.

Leakey, A. D., Uribelarrea, M., Ainsworth, E. A., Naidu, S. L., Rogers, A., Ort, D. R., and Long, S. P. Photosynthesis, productivity, and yield of maize are not affected by open-air elevation of CO2 concentration in the absence of drought. *Plant physiology*, 140(2):779–790, 2006.

Leigh, A., Sevanto, S., Ball, M. C., Close, J. D., Ellsworth, D. S., Knight, C. A., Nicotra, A. B., and Vogel, S. Do thick leaves avoid thermal damage in critically low wind speeds? *New Phytologist*, 194(2):477–487, 2012. doi:https://doi.org/10.1111/j.1469-8137.2012.04058.x.

Leigh, A., Sevanto, S., Close, J. D., and Nicotra, A. B. The influence of leaf size and shape on leaf thermal dynamics: does theory hold up under natural conditions? *Plant, cell & environment*, 40(2):237–248, 2017.

Leuzinger, S. and Körner, C. Tree species diversity affects canopy leaf temperatures in a mature temperate forest. *Agricultural and Forest Meteorology*, 146(1):29–37, September 2007. doi:10.1016/j.agrformet.2007.05.007.

Leuzinger, S., Vogt, R., and Körner, C. Tree surface temperature in an urban environment. *Agricultural and Forest Meteorology*, 150(1):56–62, January 2010. doi:10.1016/j.agrformet.2009.08.006.

Liu, S., Lu, L., Mao, D., and Jia, L. Evaluating parameterizations of aerodynamic resistance to heat transfer using field measurements. *Hydrology and Earth System Sciences Discussions*, 11 (2):769–783, 2007.

Long, S. P., Humphries, S., and Falkowski, P. G. Photoinhibition of photosynthesis in nature. *Annual review of plant biology*, 45(1):633–662, 1994.

Long, S. P., Ainsworth, E. A., Leakey, A. D. B., Nösberger, J., and Ort, D. R. Food for Thought: Lower-Than-Expected Crop Yield Stimulation with Rising CO2 Concentrations. *Science*, 312(5782):1918–1921, June 2006. doi:10.1126/science.1114722.

Maimaitijiang, M., Sagan, V., Sidike, P., Hartling, S., Esposito, F., and Fritschi, F. B. Soybean yield prediction from UAV using multimodal data fusion and deep learning. *Remote Sensing of Environment*, 237:111599, February 2020. doi:10.1016/j.rse.2019.111599.

Maseyk, K. S. *Ecophysiological and phenological aspects of Pinus halepensis in an arid-Mediterranean environment*. Ph.D., The Weizmann Institute of Science (Israel), Israel, 2006. URL https://search.proquest.com/docview/304955792/citation/84F5442BDD884B15PQ/1.

McMahon, T. A., Peel, M. C., Lowe, L., Srikanthan, R., and McVicar, T. R. Estimating actual, potential, reference crop and pan evaporation using standard meteorological data: a pragmatic synthesis. *Hydrol. Earth Syst. Sci*, 17(4):1331–1363, 2013.

Monteith, J. L. Principles of environmental physics Edward Arnold. *London, 214p*, 1973.

Muller, J. D. FLIR-A320-control: Tool to remotely focus and trigger a FLIR A320 infrared camera, October 2020. URL https://zenodo.org/record/4088156. Language: eng.

Muller, J. D. and Dingjan, T. Pine-needle-thermal-detection: Tool to detect pine needles in thermal images, November 2020. URL https://zenodo.org/record/4284621. Language: eng.

Muller, J. D. and Oz, I. Branch-chamber-fluxes: Branch-chamber-fluxes, November 2020. URL https://zenodo.org/record/4284487. Language: eng.

Muller, J. D. and Segev, L. IR-data-extraction: Tool to extract raw temperature data from FLIR R-jpegs, October 2020. URL https://zenodo.org/record/4104314.

Neriah, A. B., Assouline, S., Shavit, U., and Weisbrod, N. Impact of ambient conditions on evaporation from porous media. *Water Resources Research*, 50(8):6696–6712, 2014. doi:https://doi.org/10.1002/2014WR015523.

O'sullivan, O. S., Heskel, M. A., Reich, P. B., Tjoelker, M. G., Weerasinghe, L. K., Penillard, A., Zhu, L., Egerton, J. J. G., Bloomfield, K. J., Creek, D., Bahar, N. H. A., Griffin, K. L., Hurry, V., Meir, P., Turnbull, M. H., and Atkin, O. K. Thermal limits of leaf metabolism across biomes. *Global Change Biology*, 23(1):209–223, January 2017. doi:10.1111/gcb.13477.

Pieters, G. A. and Schurer, K. Leaf temperature measurement I. Thermocouples. *Acta Botanica Neerlandica*, 22(5):569–580, 1973.

Preisler, Y. *Water-use strategies leading to resilience of pine trees to global climatic change*. PhD Thesis, Hebrew University of Jerusalem, Rehovot, Israel, December 2019.

Qubaja, R., Grünzweig, J. M., Rotenberg, E., and Yakir, D. Evidence for large carbon sink and long residence time in semiarid forests based on 15 year flux and inventory records. *Global Change Biology*, 2019. doi:10.1111/gcb.14927.

Richardson, A. D., Aubrecht, D. M., Basler, D., Hufkens, K., Muir, C. D., and Hanssen, L. Developmental changes in the reflectance spectra of temperate deciduous tree leaves, and

implications for thermal emissivity and leaf temperature. *New Phytologist*, n/a(n/a), 2020. doi:10.1111/nph.16909.

Rotenberg, E. and Yakir, D. Contribution of Semi-Arid Forests to the Climate System. *Science*, 327(5964):451–454, January 2010. doi:10.1126/science.1179998.

Rotenberg, E. and Yakir, D. Distinct patterns of changes in surface energy budget associated with forestation in the semiarid region. *Global Change Biology*, 17(4):1536–1548, 2011. doi:10.1111/j.1365-2486.2010.02320.x.

Schuepp, P. H. Tansley Review No. 59. Leaf Boundary Layers. *The New Phytologist*, 125(3): 477–507, 1993.

Schymanski, S. J. and Or, D. Wind increases leaf water use efficiency. *Plant, Cell & Environment*, 39(7):1448–1459, 2016. doi:10.1111/pce.12700.

Schymanski, S. J., Or, D., and Zwieniecki, M. Stomatal Control and Leaf Thermal and Hydraulic Capacitances under Rapid Environmental Fluctuations. *PLOS ONE*, 8(1):e54231, January 2013. doi:10.1371/journal.pone.0054231.

Siebert, S., Ewert, F., Rezaei, E. E., Kage, H., and Graß, R. Impact of heat stress on crop yield—on the importance of considering canopy temperature. *Environmental Research Letters*, 9(4):044012, April 2014. doi:10.1088/1748-9326/9/4/044012.

Smith, W. K. Temperatures of Desert Plants: Another Perspective on the Adaptability of Leaf Size. *Science*, 201(4356):614–616, August 1978. doi:10.1126/science.201.4356.614.

Smith, W. K. Importance of Aerodynamic Resistance to Water Use Efficiency in Three Conifers under Field Conditions. *Plant Physiology*, 65(1):132–135, January 1980. doi:10.1104/pp.65.1.132.

Song, Q.-H., Deng, Y., Zhang, Y. P., Deng, X.-B., Lin, Y.-X., Zhou, L.-G., Fei, X.-H., Sha, L.-Q., Liu, Y.-T., Zhou, W.-J., and Gao, J.-B. Comparison of infrared canopy temperature in a rubber plantation and tropical rain forest. *International Journal of Biometeorology*, 61(10): 1885–1892, October 2017. doi:10.1007/s00484-017-1375-4.

Still, C., Powell, R., Aubrecht, D., Kim, Y., Helliker, B., Roberts, D., Richardson, A. D., and Goulden, M. Thermal imaging in plant and ecosystem ecology: applications and challenges. *Ecosphere*, 10(6), 2019.

Tarnopolsky, M. and Seginer, I. Leaf temperature error from heat conduction along thermocouple wires. *Agricultural and Forest Meteorology*, 93 (3):185–194, March 1999. doi:10.1016/S0168-1923(98)00123-3.

Tatarinov, F., Rotenberg, E., Maseyk, K., Ogée, J., Klein, T., and Yakir, D. Resilience to seasonal heat wave episodes in a Mediterranean pine forest. *New Phytologist*, 210(2):485–496, April 2016. doi:10.1111/nph.13791.

Tattersall, G. Thermimage, v.4.1.0, December 2019. URL https://zenodo.org/record/3590036.

Taylor, S. E. Optimal Leaf Form. In Gates, D. M. and Schmerl, R. B., editors, *Perspectives of Biophysical Ecology*, Ecological Studies, pages 73–86. Springer, Berlin, Heidelberg, 1975. ISBN 978-3-642-87810-7. doi:10.1007/978-3-642-87810-7_5.

Urban, J., Ingwers, M. W., McGuire, M. A., and Teskey, R. O. Increase in leaf temperature opens stomata and decouples net photosynthesis from stomatal conductance in Pinus taeda and Populus deltoides x nigra. *Journal of Experimental Botany*, 68(7):1757–1767, March 2017. doi:10.1093/jxb/erx052.

Verma, S. B. Aerodynamic resistances to transfers of heat, mass and momentum. *Estimation of areal evapotranspiration*, 177:13–20, 1989.

Virtanen, P., Gommers, R., Oliphant, T. E., Haberland, M., Reddy, T., Cournapeau, D., Burovski, E., Peterson, P., Weckesser, W., Bright, J., van der Walt, S. J., Brett, M., Wilson, J., Millman, K. J., Mayorov, N., Nelson, A. R. J., Jones, E., Kern, R., Larson, E., Carey, C. J., Polat, İ., Feng, Y., Moore, E. W., VanderPlas, J., Laxalde, D., Perktold, J., Cimrman, R., Henriksen, I., Quintero, E. A., Harris, C. R., Archibald, A. M., Ribeiro, A. H., Pedregosa, F., and van Mulbregt, P. SciPy 1.0: fundamental algorithms for scientific computing in Python. *Nature Methods*, 17(3):261–272, March 2020. doi:10.1038/s41592-019-0686-2.

Vishnevetsky, I., Rotenberg, E., Kribus, A., and Yakir, D. Method for accurate measurement of infrared emissivity for opaque low-reflectance materials. *Applied Optics*, 58(17):4599–4609, 2019.

Werner, C., Correia, O., Beyschlag, W., Werner, C., Correia, O., and Beyschlag, W. Characteristic patterns of chronic and dynamic photoinhibition of different functional groups in a Mediterranean ecosystem, Characteristic patterns of chronic and dynamic photoinhibition of different functional groups in a Mediterranean ecosystem. *Functional Plant Biology, Functional Plant Biology*, 29, 29(8, 8):999, 999–1011, 1011, August 2002. doi:10.1071/PP01143, 10.1071/PP01143.

Wulfmeyer, V., Branch, O., Warrach-Sagi, K., Bauer, H.-S., Schwitalla, T., and Becker, K. The Impact of Plantations on Weather and Climate in Coastal Desert Regions. *Journal of Applied Meteorology and Climatology*, 53(5): 1143–1169, January 2014. doi:10.1175/JAMC-D-13-0208.1.

Zhang, L., Niu, Y., Zhang, H., Han, W., Li, G., Tang, J., and Peng, X. Maize Canopy Temperature Extracted From UAV Thermal and RGB Imagery and Its Application in Water Stress Monitoring. *Frontiers in Plant Science*, 10, 2019. doi:10.3389/fpls.2019.01270.

Zhang, Q., Barnes, M., Benson, M., Burakowski, E., Oishi, A. C., Ouimette, A., Sanders-DeMott, R., Stoy, P. C., Wenzel, M., Xiong, L., Yi, K., and Novick, K. A. Reforestation and surface cooling in temperate zones: Mechanisms and implications. *Global Change Biology*, 26(6):3384–3401, 2020. doi:https://doi.org/10.1111/gcb.15069.